Ortega, Maray; Gómez, Daviel; Manrique, Raydel; Reyes, Guillermo; García-Sánchez, Julieth Tatiana; Baldovino Medrano, Victor Gabriel; Jiménez, Romel; Arteaga-Pérez, Luis E.

Reductive amination of phenol over Pd-based catalysts: elucidating the role of the support and metal nanoparticle size

Published in:
Reaction Chemistry and Engineering

DOI:
10.1039/d2re00259k

Published: 20/12/2022

Document Version
Peer-reviewed accepted author manuscript, also known as Final accepted manuscript or Post-print

Reaction Chemistry & Engineering

Linking fundamental chemistry and engineering to create scalable, efficient processes

Accepted Manuscript

This article can be cited before page numbers have been issued, to do this please use: M. Ortega Díaz, D. Gómez Acosta, R. Manrique, G. Reyes, J. Garcia, V. G. Baldovino Medrano, R. Jiménez and L. E. Arteaga-Pérez, *React. Chem. Eng.*, 2022, DOI: 10.1039/D2RE00259K.

This is an Accepted Manuscript, which has been through the Royal Society of Chemistry peer review process and has been accepted for publication.

Accepted Manuscripts are published online shortly after acceptance, before technical editing, formatting and proof reading. Using this free service, authors can make their results available to the community, in citable form, before we publish the edited article. We will replace this Accepted Manuscript with the edited and formatted Advance Article as soon as it is available.

You can find more information about Accepted Manuscripts in the Information for Authors.

Please note that technical editing may introduce minor changes to the text and/or graphics, which may alter content. The journal's standard Terms & Conditions and the Ethical guidelines still apply. In no event shall the Royal Society of Chemistry be held responsible for any errors or omissions in this Accepted Manuscript or any consequences arising from the use of any information it contains.

View Article Online
DOI: 10.1039/D2RE00259K

ARTICLE

Reductive amination of phenol over Pd-based catalysts: Elucidating the role of the support and metal nanoparticle size

Received 00th January 20xx,
Accepted 00th January 20xx

DOI: 10.1039/x0xx00000x

Maray Ortega[a], Daviel Gómez[b], Raydel Manrique[a], Guillermo Reyes[c], Julieth Tatiana García-Sánchez[d], Victor Gabriel Baldovino Medrano[d,e], Romel Jiménez[b], Luis E. Arteaga-Pérez[a,f]*

The heterogeneously catalyzed reductive amination of phenolics from lignin is considered an attractive sustainable route for the synthesis of primary or high-order aromatic and aliphatic amines. Here, the reductive amination of phenol with cyclohexylamine was studied, and insights into the role of the catalyst support, metal nanoparticle sizes, and acidic properties were provided. Bulk and surface characterizations, IR experiments, and kinetic measurements were performed, and their results were correlated with the catalytic performance and the content of Lewis acid sites (Pd/Al_2O_3 > Pd/C > Pd/SiO_2). The Lewis acid sites in the support and those formed by H_2 spillover assisted phenol hydrogenation and C=N bond activation, enhancing the formation of secondary amines (selectivity > 90%). The Pd coordination in the particles strongly affected the catalytic activity, indicating that phenol amination is a structure-sensitive reaction. The turnover frequency vs. dispersion profiles combined with the site distributions in the Pd particles (edge, corner, and terraces) indicate that low-coordination sites favor phenol amination, which was confirmed via diffuse reflectance infrared spectroscopy with fourier transform and high-resolution transmission electron microscopy. This study could contribute to the upcycling of fresh and recycled lignin fractions to produce aromatic and aliphatic amines.

Introduction

Secondary amines play an important role in several industries for the synthesis of fine chemicals, dyes, pharmaceuticals, and synthetic fibers.(1)·(2) The current industrial-scale secondary amine synthesis methods require strict reaction conditions, have a poor carbon economy, and produce toxic residues that represent environmental risks.(3)·(4) Therefore, sustainable secondary amine synthesis strategies based on green chemistry principles are required. In this regard, the transformation of bio-based substrates derived from lignin (e.g., aldehydes, ketones, phenols, alkenes, and alkynes) into amines has recently drawn attention (5–7). In particular, the heterogeneously catalyzed reductive amination of phenolics is considered an attractive synthesis route of primary or high-order aromatic and aliphatic amines.(8,9)

The amination of phenol proceeds via a complex mechanism involving several reaction steps, namely, hydrogenation, dehydrogenation, and condensation.(10–12) Briefly, the reaction is initiated by the hydrogenation of phenol (PhOH) to cyclohexanone (CyO), which subsequently reacts with the amine (cyclohexylamine, CyA) via a nucleophilic attack to form an intermediate imine (N-Phenylcyclohexaneimine, Imine). The imine then disproportionates to form the secondary amine. In the presence of dehydrogenating catalysts (such as Pd/C), the amine can be dehydrogenated to reduce the phenol to cyclohexanone (**Fig. 1**).

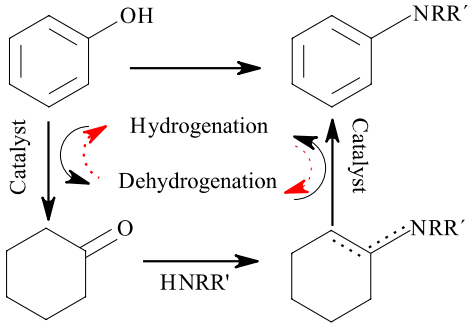

Figure 1. Summarized reaction pathway for the phenol-to-secondary amine reaction over Pd/C (adapted from(12)).

However, this reaction scheme can vary with the catalyst properties (*i.e.,* nature of the metal, metal-support interactions, support acidity, and metal nanoparticle size), phenolic nature, and reaction conditions. For example, the importance of solvents for these reactions was recently studied by Jameel *et al.*(13) The authors proved that the presence of solvents reduces the activation energy of amination, the condensation step occurs in a stepwise rather than a concerted manner. Furthermore, solvent molecules that form hydrogen bonds promote the formation of intermediates in terms of thermodynamics and kinetics by actively participating as proton transfer agents. In addition, diffusivity of hydrogen into the solvent

[a.] *Laboratory of Thermal and Catalytic Processes (LPTC), Wood Engineering Department, Faculty of Engineering, Universidad del Bio-Bio, Concepción, Chile. Email: larteaga@ubiobio.cl Twitter: @LptcUbb*
[b.] *Carbon and Catalysis Laboratory (CarboCat), Department of Chemical Engineering, Universidad de Concepción, Concepción, Chile.*
[c.] *Biobased Colloids and Materials, Department of Bioproducts and Biosystems, School of Chemical Engineering, Aalto University, FI-00076, Espoo, Finland.*
[d.] *Centro de Investigaciones en Catálisis (CICAT), Universidad Industrial de Santander, Colombia*
[e.] *Laboratorio Central de Ciencia de Superficies (SurfLab), Universidad Industrial de Santander, Colombia*
[f.] *Universidad de Concepción, Unidad de Desarrollo Tecnológico, UDT, Coronel, Chile*

is critical to facilitate its access to the catalyst´s active sites, thus, to complete the catalytic cycle.

Chen *et al*. (11,14) explored the direct cross-coupling of phenols of aniline at temperatures in the range of 80–120 °C. They demonstrated that transition metal complexes (Rh, Pt, Ru, Ni, and Ir) do not produce any aromatic amines, while Pd/C can lead to a 94% yield of arylamine. More recently, Tomkins *et al*.(15) demonstrated that Rh/C can convert 98% of the phenol to cycloheyxlamine with a selectivity of 98%, while the dehydrogenation over Pd leads to a 41% yield of N-substituted anilines. In a later study from the same group, Cuypers *et al*.(16) suggested that the acidity of the support plays a major role in the hydrogenation and condensation of cyclohexanone with amino groups. Nonetheless, the nature of the surface acid sites (Lewis or Brønsted) and the role of the metal nanoparticle size in the reaction were not considered. These aspects were studied by Vidal *et al*.(17) using Pt/TiO_2 and ethyl levulinate. They concluded that a high Pt dispersion and the $Pt\text{-}TiO_2$ interphase favored the spillover of dissociated hydrogen, generating protonic acid sites, thus increasing the rate of imine formation. On the other hand, Corma *et al*.(18) verified that the hydrogenation of imines is sensitive to the Pd nanoparticle structure, and that the activity and selectivity increase with Pd dispersion. They proposed that small metal particles, where step and corner sites are relatively abundant, are more favorable for the cleavage of C–O bonds than large metal particles, which have abundant terrace sites. Similarly, Mazarío *et al*.(19) observed that the average Pd particle size in the catalyst increased slightly after several reaction cycles, leading to a reduced activity. However, an apparent contradiction was proposed by Resende *et al*.,(20) who observed low activities for small Pd metal nanoparticles and attributed this to interactions with reactive substrates. Although these studies focused on the particle size and nature of the catalyst, they suggested that the reaction performance can be significantly affected by the metal-support interactions or support properties. In addition, the nature of the acidic sites plays a key role in the hydrogenation of the N=C bonds. Hattori and Shishido(21) demonstrated that hydrogen can be dissociatively adsorbed on Pt sites to form hydrogen atoms, which migrate to the Lewis acid sites of the support and participate in the hydrogenation. Similar results were reported by Santoro *et al*.,(22) who aimed to simplify the number of steps in the reductive amination of aromatic ketones on Cu catalysts supported on SiO_2, Al_2O_3, and TiO_2. They prepared multifunctional catalysts with tailored densities of acidic and hydrogenation-active sites by changing the catalyst support. A Cu/SiO_2 catalyst was active as a Lewis acid catalyst in its non-reduced form and very active for the selective hydrogenation in its reduced form, effectively promoting the direct reductive amination of aromatic ketones. Recently, Mazarío *et al*.(19) investigated the role of the support acidity and nanoparticle size using metal oxides (TiO_2, Al_2O_3, ZrO_2, and MgO) and their mixtures ($TiO_2\text{-}Al_2O_3$, $TiO_2\text{-}ZrO_2$, and $ZrO_2\text{-}Al_2O_3$) as supports for Pd nanoparticles. They demonstrated that a high density of acid sites resulted in the formation of undesirable nitrogen-containing sub-products. Furthermore, it was found that the presence of a large number of unsaturated Pd sites on the surface is essential for activating the C=N bond and enhancing its hydrogenation. However, the relationship between the nature of the acidic sites and the reaction behavior is yet to be clarified.

Although the previously discussed studies suggest that the quantity and nature of the acid sites in the support and the coordination degree of the metal nanoparticles are key parameters for reductive amination processes, there is no consensus on their specific roles in phenol amination. Moreover, different carbon-containing substrates (phenolic, alcohol, or ketone) and amines (NH_3, aniline, or cyclohexylamine) could lead to different surface interactions, as extensively revised by Gomez *et al*.(23).

Le Valant *et al*.(24) suggested that a decrease in the catalyst particle size could enhance the effect of the support by modifying the electronic properties of the metal nanoparticles or increasing the contact area between the metal crystallites and the support. These effects have been reported for amination and hydrogenation reactions; thus, it is plausible that the phenol-to-secondary amine reaction is affected by the metal dispersion (17,19,25).

In this study, we investigated the role of the metal nanoparticle size and catalyst support in the amination of phenol over supported Pd catalysts. Pd was used as a reference metal because of its proven activity in amination processes. Activated carbon, SiO_2, and Al_2O_3 were selected as supports owing to their abundance, industrial relevance, and different metal-support interactions. All the materials were extensively characterized, and their structural, chemical, and physical properties were correlated with the reaction performance.

Materials and Methods

Synthesis and characterization of the catalysts

Commercial 10% Pd/C (CAS-87104) was obtained as an oxide from Merck Group (Chile). Pd/SiO_2 and Pd/Al_2O_3 were prepared via incipient wetness impregnation of the supports (SiO_2, Sigma-Aldrich, CAS-112926-00-8 and Al_2O_3, Sigma-Aldrich, CAS-1344-28-1) with suitable volumes of a $PdCl_2$ solution (59%, Sigma-Aldrich, CAS-7647-10-1) at a controlled pH (~1.5), and using triethanolamine (TEA, ≥ 99.0%, Merck, CAS-102-71-6) to achieve a homogeneous metal dispersion.(26) The catalysts were then calcined at 500 °C for 4 h to remove the remaining TEA and produce oxidized precursors. The calcination conditions were determined via thermogravimetric analysis (TGA-MS, STA 409 PC, Netzsch) coupled with mass spectrometry (QMS 403C Aëolos, Netzsch), using specific m/z signals (m/z: H_2O (18), NO_2 (30), and CO_2 (44)) as oxidation tracers. The thermal stability of the catalysts for the reaction temperatures was also confirmed (< 5% weight loss below 200 °C).

According to Van Santen(27) for particle sizes ranging between 2 and 20 nm, three reaction rate behaviors can be observed: (i) reaction rates that increase when the particle size decreases, (ii) reaction rates that decrease with a decrease in particle size, and (iii) reaction rates that are independent of the particle size. This is the basis for classifying reactions as structure-sensitive or structure-insensitive. Different Pd/Al_2O_3 metal nanoparticles sizes (in the range of 2–10 nm) were obtained by changing the metal loading (1%, 5%, and 10% wt./wt.) and the thermal treatment conditions. These samples were denominated $Pd/Al_2O_3\text{-}Di$, where Di represents the average nanoparticle size (i = 1–4, from lowest to highest nanoparticle size).

The morphology and composition of the catalysts were investigated using scanning electron microscopy (SEM) and energy-dispersive X-ray spectroscopy (EDX), respectively. The analyses were performed using a Hitachi SU3500 device operated at an acceleration voltage of 20 kV and coupled with a Bruker XFlash 610M EDX accessory for semi-quantitative spectral analysis.

The metal content in the samples was inspected by atomic absorption spectrometry (AAS) in a Perkin Elmer 3100 instrument (Perkin Elmer, Manasquan, NJ, USA). Prior to the analyses the

samples were subject to microwave-assisted digestion using 50 mg of the catalyst and 10 mL of concentrated HNO_3/HCl (See Table E1).

Temperature-programmed reduction (TPR) experiments were performed using a Micromeritics ASAP 2010 device equipped with a TCD cell to quantify the H_2 consumption. The total acidity was measured via temperature-programmed desorption of ammonia (NH_3-TPD) using a 3FLEX device (Micromeritics) equipped with a TCD and combined with a mass spectrometer (Cirrus 2, MKS Instruments).

The specific surface areas and pore volumes were calculated from N_2 adsorption–desorption isotherms at 77 K using the Brunauer–Emmett–Teller (BET) model and Barrett–Joyner–Halenda (BJH) method, respectively. Both isotherms were recorded using a 3FLEX instrument (Micromeritics). Before the analysis, the samples were degassed during 24 h under vacuum at 150 °C.

The bulk crystalline phases were analyzed via X-ray diffraction (XRD) using a Bruker D4 Endeavour diffractometer with Cu Kα radiation (λ = 0.15418 nm). The scanning was performed between 3° and 90° 2θ at a speed of 0.02°/s using a signal generated at 40 kV and 20 mA. The crystalline phases were identified via a search-match procedure with the Mercury 3.7 software, using the Crystallography Open Database. the metallic particle sizes were estimated using the Scherrer equation (Eq. 1)(28):

$$L = \frac{K * \lambda}{\beta * cos\,(\theta)} \qquad (1)$$

where L is the crystallite size in nm, λ is the Cu Kα wavelength in nm, β is the full width at half maximum (FWHM) of the main peak in radians, K is a constant close to unity, and θ is Bragg's angle in radians.

Transmission electron microscopy (TEM) images were obtained using a JEOL JEM 1200 EXII microscope at 120 kV. Transmission electron microscopy (TEM) images were obtained using a JEOL JEM 1200 EXII microscope at 120 kV. For this measurement, the catalysts were dispersed in ethanol in an ultrasound bath for approximately 5 min, deposited on carbon-coated copper grid, and air-dried before imaging. The images were processes with the software Image J and the particle size distribution was estimated from the average of 5 to 10 TEM images using the volume-weighted function recommended by Vannice (Eq.2)(29):

$$dp_i = \frac{\sum_{j=1}^{n} n_j \times {d_{pj}}^4}{\sum_{j=1}^{n} n_j \times {d_{pj}}^3} \qquad (2)$$

The images were processed using the ImageJ software to obtain the particle size distributions (particle count: approximately 90–100). Finally, the metal dispersion was calculated from the average particle size assuming a hemispherical shape (Eq. 3).

$$D = \frac{6 \times \left({}^{v_m}/_{a_m}\right)}{dp} \qquad (3)$$

where D is the metal (Pd) dispersion, v_m is the volume occupied by an atom in the bulk metal (for Pd: 14.7 Å^3), a_m is the area occupied by a surface atom (for Pd: 7.93 Å^2), and dp is the average nanoparticle size obtained from the TEM analysis.

High-resolution transmission electron microscopy (HRTEM) images and electron diffraction patterns were acquired using a JEOL JEM-2200FS (JEOL, Mitaka, Tokyo) microscope with double aberration correction, operated at an acceleration voltage of 200 kV. The samples for the HRTEM studies were drop-cast with acetone onto Cu grids coated with an ultrathin holey carbon film.

The nature of the surface acid sites was investigated via Fourier-transform infrared (FTIR) spectroscopy with pyridine (C_5H_5N, J.T. Baker, > 99.9% purity) in a flow cell equipped with ZnSe windows and a vacuum system (Pfeiffer HiCube Eco Turbo). IR spectra at different desorption temperatures were collected with a Nicolet iS50 device (Thermo Scientific) using an MCT detector and 32 scans with a resolution of 4 cm^{-1}. Diffuse reflectance Fourier transform infrared spectroscopic (DRIFTS) measurements of the CO adsorption on Pd/Al2O3-Di (i = 1 to 4) were performed for to relate Degree of surface coordination as a function of particle size. The technique is described in further detail in the *Supplementary Material*.

Catalytic tests

The reagents were acquired from Merck Group (Chile) as analytical standards. The imine (> 95%, CAS-1132-38-3) was synthesized and provided by AKos GmbH, Ukraine. Tert-amyl alcohol (> 95%; CAS-75-85-4, Sigma Aldrich, Chile) was used as the solvent for the reactions.

The reaction tests were performed in reinforced glass autoclave reactors (4 mL) equipped with a H_2 line for pressurization. The reactors were placed in a Reacti-Therm™ system (Thermo Fisher, USA) equipped with an external thermocouple and magnetic stirring. To measure the concentrations over time, the reactant quantities were increased by a factor of 15, and the reaction was performed in an SS316 autoclave reactor (20 mL) equipped with a polytetrafluorethylene liner and a sampling port.

Identification and quantification of the products

The products were analyzed using a gas chromatograph (Clarus 690, PerkinElmer) equipped with a mass spectrometer (QS8, PerkinElmer), and the compounds were identified by comparing their ionization patterns (m/z range: 30–600 Da) with the standard spectra database of the NIST library. The products were quantified using a gas chromatograph (8610, SRI Instruments) equipped with an on-column injection port and a flame ionization detector. The separation of analytes was achieved with an MTX-5 column (30 m x 0.25 mm x 0.1 µm) and the retention times were assigned by injecting solvent-pure samples prior to the product analysis. The quantification was performed using nonane as an internal standard.

Conversion of reactants (amine and phenol) and selectivity of products (based on GC-FID measurements) were defined as: (initial moles of reactant−final moles of reactant)/initial moles of reactant×100), and (moles of product i)/moles of total products×100, respectively. Turnover frequency (TOF) was defined as: (moles of product i)/(moles of surface metal in the catalyst).

Experimental plan

The experimental conditions used for the study of phenol amination with cyclohexylamine using different catalyst supports and metal nanoparticles sizes are listed in the *Electronic Supplementary Material* (**Table E2**). These conditions eg., tert-Amyl alcohol (TAA) solvent, H_2 pressure, temperature and reactants initial concentrations were selected inspired in previously published papers(30,31) and in a preliminary screening performed for Pd/C. The data of this screening can be accessed in a Mendeley data repository(32). All the measurements were performed under a

kinetically controlled regime, which was confirmed here by the application of the Weisz-Prater and Mears´ criteria(29).The details of these calculations are also provided in the ESI (**Tables E3** and **E4**). The tert-amyl alcohol was used as solvent owing to its nucleophilic properties that favor proton transfer (relevant for hydrogenation steps) and because it is friendly to the environment, which makes it a strong candidate for green amines productions.

Finally, the basic reaction conditions where: reaction time = 20 h, T = 140 °C, p_{H2} = 1.5 Bar, C^0_{PhOH}, C^0_{CyA} = 1.4 Eq., Pd/C 5% mol/mol with respect to phenol, a stirring speed of 900 rpm and tert-amyl alcohol as solvent.

Results and Discussion

Surface characterization of Pd/C, Pd/Al_2O_3, and Pd/SiO_2

The SEM micrographs and detected EDX signals suggest a uniform surface distribution of Pd on the three supports (See **Fig. E1** in Supplementary Material). The signals from the linear EDX atomic scan and the results from atomic absorption analyses confirmed that the Pd loadings achieved via incipient wetness impregnation were in the same order as the theoretical Pd loadings for Pd/C, Pd/Al_2O_3, and Pd/SiO_2. The values of metal content measured by AAS were used for the estimation of turnover frequency and other quantitative parameters involving catalyst composition. **Figs. 2a** and **2b** show that the textural properties of Pd/SiO_2 and Pd/Al_2O_3-D3 are similar in terms of surface areas (219 – 221 m^2/g), pore volumes, and pore sizes (see **Table 1**). However, the Pd/C catalyst showed a higher surface area (832 m^2/g) and lower average pore size than those of Pd/SiO_2 and Pd/Al_2O_3-D3. Despite these differences, the shapes of the N_2 adsorption–desorption isotherms suggest that all the samples were mesoporous materials (**Fig. 2a**) with narrow pore size distributions. In particular, the isotherms for Pd/SiO_2 and Pd/Al_2O_3-D3 show hysteresis loops closing approximately at p/p_0 = 0.4, which is associated with type IV isotherms according to IUPAC.

The Pd/C catalyst stands out in terms of its high surface area and narrow pores, whereas the Pd/SiO_2 and Pd/Al_2O_3-D3 catalysts appear to be similar. Therefore, any significant difference in performance between the SiO_2 and Al_2O_3 catalysts can be attributed to the support-Pd interactions. The differences in nature of the supports makes their physicochemical study essential, because it can provide relevant information about their role in the phenol amination reaction.

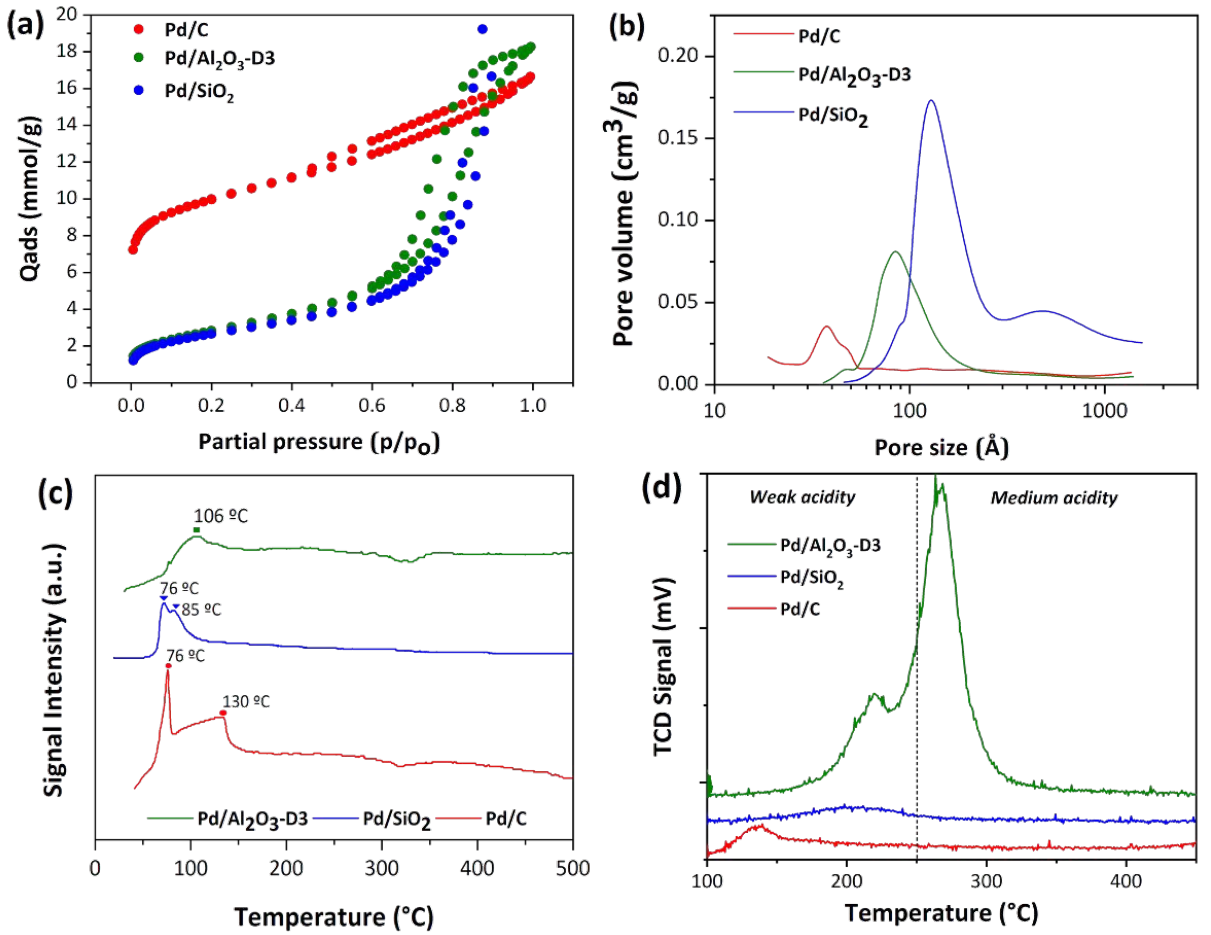

Figure 2. Surface and textural characterization of the Pd/C, Pd/Al_2O_3, and Pd/SiO_2 catalysts. (a) N_2-Physisorption isotherms, (b) pore size distributions, (c) temperature programmed reduction profiles, and (d) temperature programmed desorption of ammonia profiles. **Note:** Analysis performed after catalysts reduction (The TPR was performed for calcined samples prior to reduction).

The TPR profiles for the calcined Pd/C, Pd/Al_2O_3-D3, and Pd/SiO_2 catalysts are shown in **Fig. 2c**. For Pd/C and Pd/SiO_2, a high-intensity reduction peak was observed at low temperatures (approximately 76 °C), which can be attributed to the formation of palladium β hydrides after the reduction of small PdO nanoparticles.(33–36) Furthermore, attenuated signals were observed for the three catalysts between 85

and 130 °C. These peaks can be attributed to the reduction of Pd^{2+} to Pd^0 at low temperatures, indicating the presence of small nanoparticles with a narrow distribution.(37–40) The similar TPR profiles indicate that the three materials should be reduced under the same conditions to achieve a predominance of Pd^0 nanoparticles and similar particle size distributions. This hypothesis was further confirmed via TEM and XRD.

Finally, the total concentrations of acidic sites and their relative strengths on the Pd/C, Pd/Al_2O_3-D3, and Pd/SiO_2 catalysts are shown in **Fig. 2d**. The strength of the acidic sites was determined according to the temperature of the corresponding ammonia desorption peak: weak, medium, and strong acidic sites correspond to temperatures below 250 °C, between 250 and 450 °C, and above 450 °C, respectively.(41) Interestingly, the three catalysts showed desorption peaks at temperatures below 250 °C, indicating the presence of weak acidic sites, which were predominant in Pd/SiO_2. The Pd/Al_2O_3-D3 catalyst showed an additional high-intensity desorption peak located between 250 and 300 °C, indicating that the sites with medium acidity were predominant in this material. The evolved gases from these tests were analyzed to confirm the signals attributable to N_2 and NH_3 (**Fig. E2** in Supplementary Material). For all catalysts, the reduction peaks at low temperatures were correlated with the desorption of molecular ammonia, indicating that it was weakly adsorbed (likely physiosorbed) on the weak acidic sites. However, at temperatures above 250 °C, the reduction peaks correlated with the signals of NH_3 (m/z = 17) and N_2 (m/z = 14, 28). This last result was observed for Pd/C and Pd/Al_2O_3-D3 and suggests that strongly adsorbed ammonia molecules undergo a redox decomposition with surface O sites, as previously reported.(42–44)

The TPD-NH_3 results indicate that the three catalysts have different concentrations of superficial acidic sites of different nature, which is necessary to investigate their role in the reductive amination of phenol.

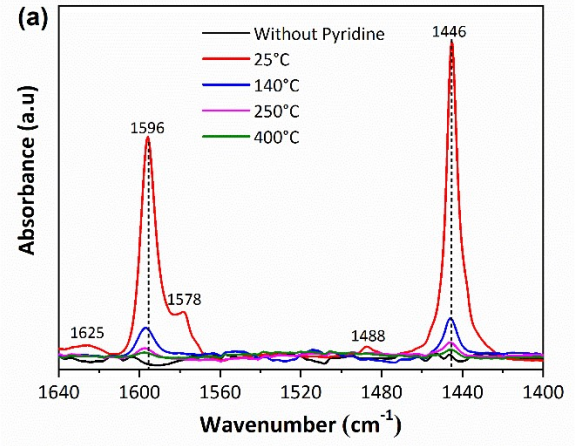

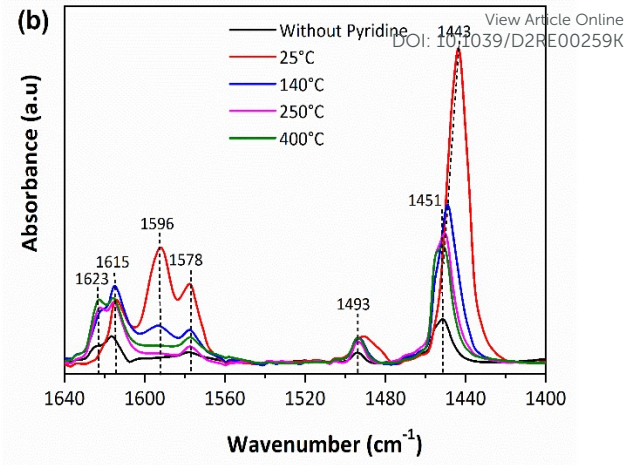

Figure 3. Fourier-transform infrared spectra of pyridine desorbed at 25, 140, 250, and 400 °C from Pd catalysts (10% wt./wt.) on (a) SiO_2 and (b) Al_2O_3 supports. **Note:** Analysis performed after catalysts reduction.

The nature of the surface acidic sites of these catalysts was studied via adsorption/desorption of pyridine assisted by FTIR spectroscopy (**Fig. 3**). The Pd/SiO_2 catalyst shows two main peaks at 1446 and 1596 cm^{-1} associated with coordinated pyridine at Lewis acid sites; this is typically seen in silica-based catalysts.(45–48) The Pd/Al_2O_3-D3 catalyst shows additional peaks at 1493, 1578, 1615, and 1623 cm^{-1} that can be attributed to the coordination of pyridine at Lewis acid sites.(47,49) In the Pd/Al_2O_3 catalyst, the Lewis sites correspond to exposed Al^{3+} sites and are classified as medium (1578–1596 cm^{-1}) and strong acidic sites (1615–1623 cm^{-1}).(47,50,51) The FTIR-PyR confirmed the absence of signals at 1545 cm^{-1}, which indicates that none of the catalysts contains Brønsted acid sites.(45,47) The Lewis acidity of Pd on the SiO_2 and Al_2O_3 catalysts can be determined by comparing the intensities of the peaks at 1446 cm^{-1}. The concentrations of acidic sites were calculated from the experiments at 140 °C by applying the molar extinction coefficient for the peak at 1446 cm^{-1} (2.22 cm μmol^{-1}), determined by Emeis.(52) The Pd/Al_2O_3-D3 catalyst exhibited the highest concentration of Lewis acid sites (371 µmol g_{cat}^{-1} vs. 95 µmol g_{cat}^{-1} for Pd/SiO_2) and abundant strong Lewis acid sites, corresponding to the range of 1615–1623 cm^{-1}. The ratio of intensities at 1446 cm^{-1} $\left({}^{A_{Pd/Al_2O_3-D3}}/_{A_{Pd/SiO_2}}\right)$ indicates that the acidity of the Pd/Al_2O_3-D3 catalyst is approximately 3.9 times higher than that of Pd/SiO_2. On the other hand, the carbon support of the Pd/C catalyst used in this study was identified by Wu *et al.*(53) as an acidic material, with a predominance of Lewis acid sites (151 µmol g_{cat}^{-1}). This is mainly because the carbon support is electrophilic.(53–55) In addition, the interactions between Pd and the acid sites forms an electron-deficient structure, which can also result in Lewis acidity.

Structural and morphological properties

The XRD patterns of the Pd/C, Pd/Al_2O_3-D3, and Pd/SiO_2 catalysts (**Fig. 4a)** show five diffraction peaks centered at 40.0°, 46.7°, 68.1°, 82.2°, and 86.7°. These reflections were respectively attributed to the (111), (200), (220), (311), and (222) planes of metallic Pd with a face-centered cubic structure (fcc)(33–36,56–60). For the Pd/C catalyst, the weak signal close to 30.0° can be attributed to the amorphous carbon support, whereas the Pd/SiO_2 catalyst presented a diffraction peak at approximately 22.6° that corresponds to amorphous silica. The Pd/Al_2O_3-D3 catalyst mainly showed

characteristic diffraction peaks of the support (γ-Al_2O_3) at 37.7°, 39.4°, 45.8°, 60.8°, 66.9°, and 84.8°, while the Pd signals could only be detected at 40.0° and 82.2°owing to the diffraction peaks of Pd and Al_2O_3 overlapping. The absence of diffraction peaks at 33.9°, 42.0°, 54.8°, and 73.9°, corresponding to the (101), (110), (112), and (211) planes of PdO, respectively,(61,62) suggests that the reduction treatment was effective in predominantly generating Pd^0 sites on the surface.

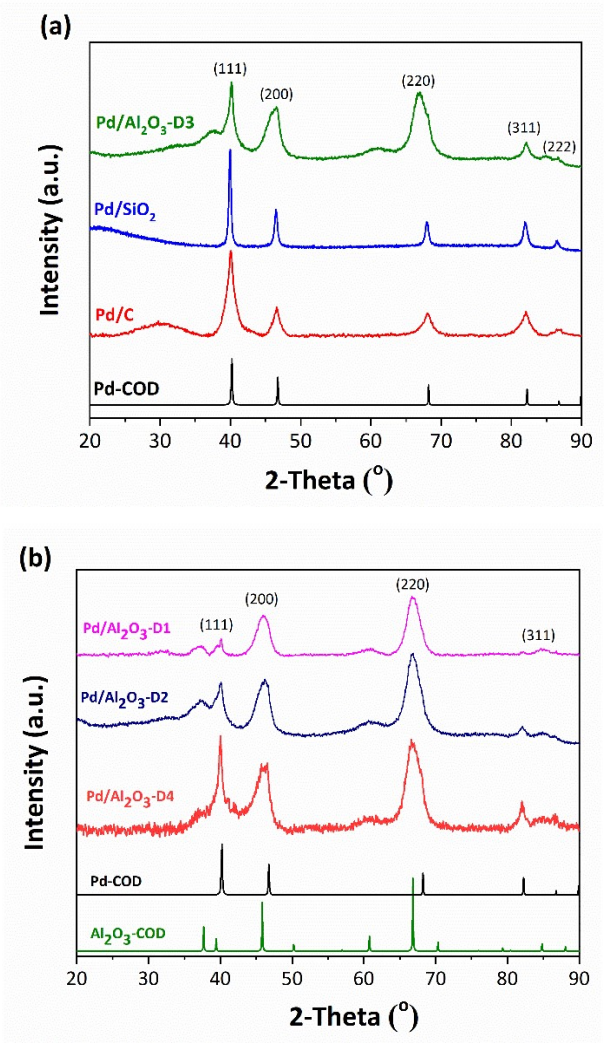

Figure 4. (a) X-Ray diffraction (XRD) patterns for Pd on different supports (Pd/C, Pd/Al_2O_3-D3, and Pd/SiO_2). (b) XRD patterns for Pd with different metal nanoparticles sizes (D1, D2, D4) supported on Al_2O_3. Standards from the Crystallography Open Database are shown:(60) Pd (1011105) and Al_2O_3 (2107301). **Note:** Analysis performed after catalysts reduction.

Fig. 4b shows the XRD spectra of the three other Pd/Al_2O_3 catalysts with different particle sizes (Pd/Al_2O_3-D1, Pd/Al_2O_3-D2, and Pd/Al_2O_3-D4). These patterns and those of Pd/Al_2O_3-D3 show different intensities of the diffraction peaks at 40.0°, 82.2°, and 86.7° that correspond to Pd^0, while the Pd peaks at 46.7° and 68.1° overlapped with the signals at 45.8° and 66.9° of the (400) and (440) planes of Al_2O_3. The Pd/Al_2O_3-D1 catalyst was the most complex to analyze because of its low Pd content (approximately 1% wt./wt.) and the peaks of Pd and Al_2O_3 overlapping, which hinders Pd quantification.

The Pd crystallite sizes were calculated using the Scherrer equation applied to the reflection at 40°. The results are listed in **Table 1**.

Figs. 5a to **5c** show the TEM images and the corresponding particle size distribution histograms of Pd/C, Pd/Al_2O_3-D3, and Pd/SiO_2. **Figs. 5d** to **5f** show the results for the three additional Pd/Al_2O_3 catalysts prepared with different metal nanoparticles sizes (Pd/Al_2O_3-D1, Pd/Al_2O_3-D2, and Pd/Al_2O_3-D4).

The TEM images show particles with well-defined contours that are dispersed on the supports. This suggests that the use of TEA during the incipient wetness impregnation effectively contributed to the formation of uniformly distributed Pd nanoparticles with unimodal size distributions, with standard deviations of less than 1.1 nm. The similar dispersions found for Pd/C (33%), Pd/Al_2O_3-D3 (30%), and Pd/SiO_2 (24%) are suitable for studying the effect of the support on the catalytic amination of phenols without significant interference from the previously reported structural sensitivity (17). Finally, the TEM images shown in **Figs. 5d** to **5f** confirm the effectiveness of the synthesis method used to produce different particle sizes in Pd/Al_2O_3-D1 (1.7 nm), Pd/Al_2O_3-D2 (2.3 nm), and Pd/Al_2O_3-D4 (7.7 nm). According to Van Santen,(27) the reactivity of the metal particles can be correlated to their orbital structure, which is strongly affected by the number of atoms. For particles between 1 and 3 nm, the number of surface atoms is higher than the number of bulk atoms; at 3 nm, the number of surface atoms becomes lower than the number of bulk atoms. Therefore, the particle sizes shown here (1–10 nm) are in a range which allows us to investigate the relevance of the structural sensitivity in the phenol amination process.

Table 1. Characterization results for the Pd/C, Pd/SiO_2, and Pd/Al_2O_3. **Note**: Analysis performed after catalysts reduction.

Catalyst	Density of acidic sites (10^{-3}μmol$_{NH3}$/ m$^2_{cat}$)			
	Weak	Medium	Strong	Total
Pd/C	1.1	N.D.	-	1.1
Pd/SiO_2	2.8	N.D.	N.D.	2.8
Pd/Al_2O_3-D3	48	54	N.D.	100

Catalyst	Particle size[a] (nm)	Particle size[b] (nm)	Surface area (m²/g)	Dispersion (%)	Pore size (nm)
Pd/C	5.8	3.3±1.1	832	33	2.8
Pd/SiO_2	8.6	4.6±1.0	219	24	16.4
Pd/Al_2O_3-D3	6.6	3.6±0.7	221	30	10.8
Pd/Al_2O_3-D4	9.6	7.7±0.5	-	14	-
Pd/Al_2O_3-D2	5.6	2.3±0.7	-	47	-
Pd/Al_2O_3-D1	4.5	1.7±0.4	-	64	-

[a] Derived from the Scherrer equation (Eq. 1)

[b] Determined from TEM micrographs, used to determine D_i (Eq. 2)

The particle size overestimation by the Scherrer equation (with respect to the particle size measure via TEM) can be attributed to any type of lattice imperfection that causes additional diffraction line broadening. Therefore, the metal particle size measured using X-ray diffraction is rarely equivalent to that measured via microscopic methods.(63–65) Despite the TEM technique could also imply some deviations from actual size values, it is more accurate than XRD, thus the dispersions calculated via TEM were used here for the quantification of the reaction rates expressed as turnover frequency (TOF).

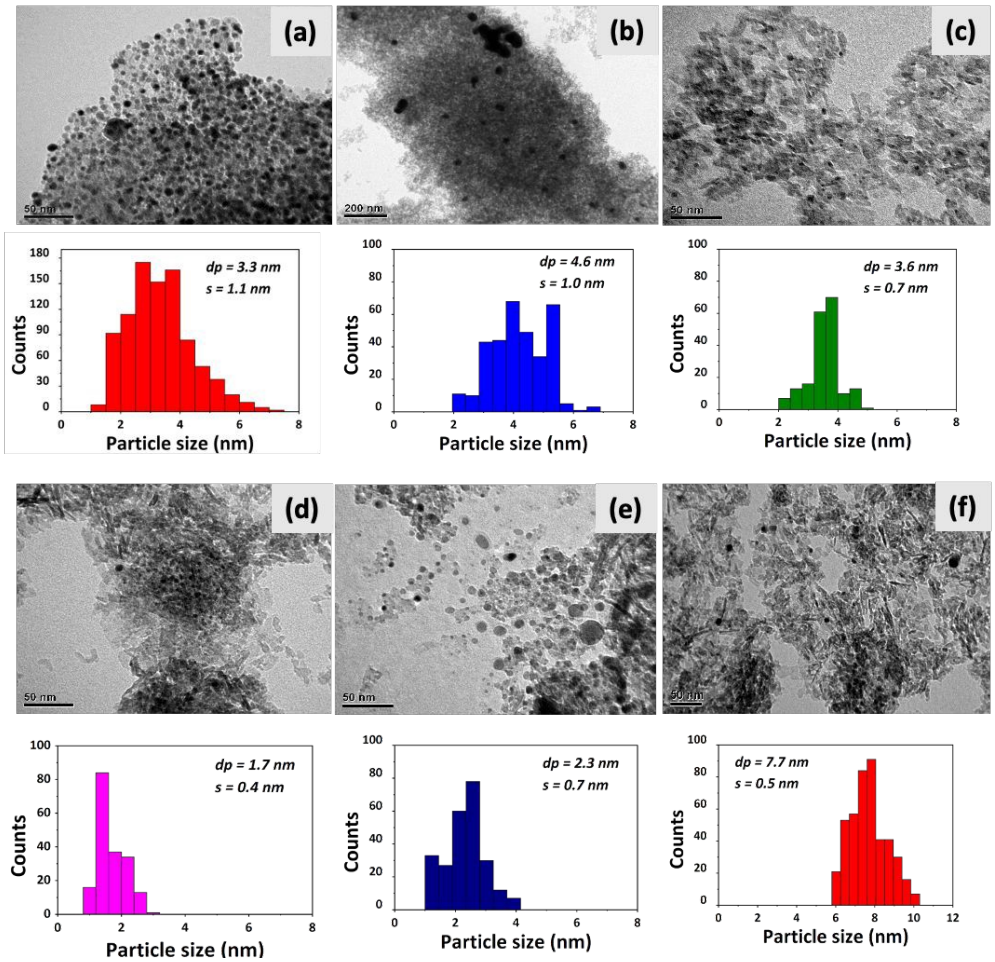

Figure 5. Transmission electron microscopy images and their corresponding particle size distributions for (a) Pd/C, (b) Pd/SiO_2, (c) Pd/Al_2O_3-D3, (d) Pd/Al_2O_3-D1, (e) Pd/Al_2O_3-D2, and (f) Pd/Al_2O_3-D4. dp: average particle size; s: standard deviation. **Note:** Analysis performed after catalysts reduction.

HRTEM and selective area diffraction measurements were used to characterize the Pd with different particle sizes on Al_2O_3 surfaces (**Fig 6**). The electron diffraction patterns shown in the lower left corner of each image exhibit three diffuse rings, which can be assigned to the (111), (200), and (311) planes of fcc palladium. The interplanar distances calculated from the (111) rings are consistent with those reported by other authors (66–68).

The HRTEM images show that the synthesized Pd nanocrystals mainly display octahedral geometries. The octahedral particles exhibit the expected (111) facet(67) with multiple dislocations on this plane. The lattice spacing of the measured fringes was larger for the Pd/Al_2O_3-D1 catalyst (d = 0.35 nm) than for the other catalysts. In general, the Pd nanoparticle surface analyses show that the differences are mainly attributed to surface facets.

View Article Online
DOI: 10.1039/D2RE00259K

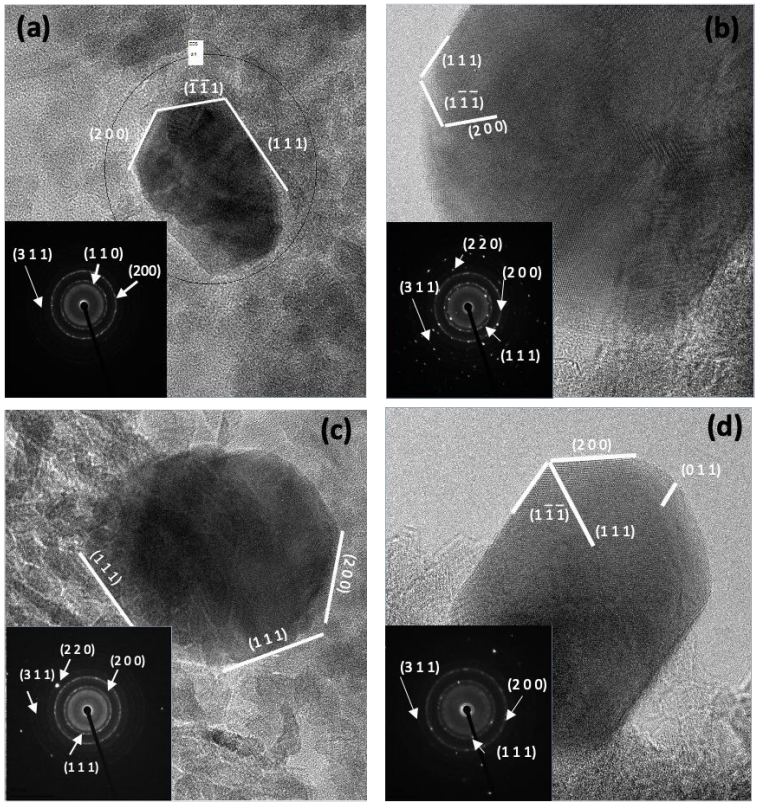

Figure 6. High resolution transmission electron microscopy images of (a) Pd/Al_2O_3-D1, (b) Pd/Al_2O_3-D2, (c) Pd/Al_2O_3-D3, and (d) Pd/Al_2O_3-D4. Insets: electron diffraction patterns. **Note:** Analysis performed after catalysts reduction.

Catalytic experiments

Elucidation of the reaction pathways

Preliminary activity measurements and time-dependent experiments were performed to propose a reaction pathway for phenol reductive amination. The experimental plan includes a set of experiments designed to eliminate the homogeneous reaction contribution and intrinsic activity of the supports (runs 1–6 in **Table 2**).

The experiments in non-catalytic conditions (**run-1**) and with the Al_2O_3 support (**run-2**) confirmed that the homogeneous condensation between phenol and cyclohexylamine occurs at a very low reaction rate (0.0008 mmol/h) and yields the intermediate imine as a product.(17,23,69) When the carbon support was used (**run-3**), the phenol conversion was similar to that of run-1, but cyclohexanone was detected in the products, which suggests the occurrence of phenol hydrogenation with this support. Finally, the phenol conversion with SiO_2 (**run-4**) was zero; however, the cyclohexylamine conversion with SiO_2 was 9%, and imine was the only product (**run-4**), which suggests that the amine underwent self-condensation with this support. The phenol conversion values obtained for the homogeneous reaction conditions and with the three supports, this is, **run-1** to **run-4** (< 6% after 20 h), demonstrate that the substrate-surface interactions and the presence of a metal catalyst are critical for achieving a reasonable activity level for this reaction system. The effectiveness of Pd^0 for hydrogenation and amination was confirmed by the results of **run-5** to **run-7**. The results from **run-6** confirmed the total conversion of phenol (X_{PhOH} = 100%) via its partial hydrogenation to cyclohexanone on Pd/C. However, the reduction of the produced cyclohexanone to cyclohexanol over Pd^0 was hindered, presumably owing to the keto-enol equilibrium between cyclohexanone and a surface intermediary, which is the kinetically relevant step in this reaction.(70,71) This is a remarkable result because the over-hydrogenation of phenol would reduce the effectiveness of the amination cycle. Self-condensation of the amine (**run-6**) to form dicyclohexylamine (DCyA) and cyclohexylaniline (CyPhA) was observed. This confirmed the capacity of Pd^0 to promote the hydrogenation/dehydrogenation of the intermediate imine. This capacity was further studied via a reaction experiment in the absence of H_2 (**run-7**). The selectivity of the dehydrogenated secondary amine (CyPhA) was 1.7 times that of dicyclohexylamine. These results suggest that the Pd^0 sites can promote the dehydrogenation of the imine, providing the necessary H_2 equivalents to complete the catalytic cycle, as has been previously reported for a similar reaction.(72) Finally, the Pd/C catalyst demonstrated remarkable activity in the amination of phenol with cyclohexylamine (**run-8**), mainly producing dicyclohexylamine, cyclohexylaniline, and cyclohexanone. Based on these results, we proposed a reaction pathway for the amination of phenol with cyclohexylamine (**Fig. 7**).

The reaction begins with the hydrogenation of phenol to cyclohexanone, which subsequently reacts with the amine (cyclohexylamine, CyA) via a nucleophilic attack to form an intermediate imine (cyclohexaneimine, Cy=NCyA). The imine then disproportionates to form secondary amines (dicyclohexylamine, DCyA, and/or cyclohexilaniline, CyPhA). In addition to this main reaction cycle, we propose that parallel self-condensation of the CyA via a hemi-aminal intermediate could occur, producing DCyA and NH_3. The DCyA can then be dehydrogenated to produce CyPhA. The species involved in this cycle and reported in Table 2 were identified via gas chromatography coupled to mass spectrometry,

and their analytical standards were used for quantification (See ESI_2.xls and ESI_3.xls). Despite, several authors having proposed the hemi-aminal as an intermediary for these reactions, it is very reactive and unstable under the reaction conditions used here, thus it was not detected by GC-MS (15,73–76).

Table 2. Preliminary assays. Reactions were performed in 4 mL glass autoclaves, using tert-amyl alcohol as solvent during 20 h at 140 °C.

Run	Catalyst	Phenol (mol/L)	Cyclohexylamine (eq.)	H_2 (bar)
1	**n.n.**	0.20	1.40	1.5
2	Al_2O_3	0.20	1.40	1.5
3	C	0.20	1.40	1.5
4	SiO_2	0.20	1.40	1.5
5	Pd/C	**0.0**	1.40	1.5
6	Pd/C	0.20	**0.0**	1.5
7	Pd/C	0.20	1.40	**0.0**
8	Pd/C	0.20	1.40	1.5
		Results*		
Run	**X_{PhOH}/X_{CyA} (%/%)**	**S_{DCyA} (%)**	**S_{CyPhA} (%)**	**S_{CyO} (%)**	**S_{Imine} (%)**
1	3/5	n.d.	n.d.	n.d.	100
2	3/3	n.d.	n.d.	n.d.	100
3	6/8	n.d.	n.d.	10	90
4	0/9	n.d.	n.d.	n.d.	100
5	24	77	23	n.d.	n.d.
6	100	n.d.	n.d.	100	n.d.
7	15/76	36	61	n.d.	3
8	87/78	57	18	24	1

$X_i = 100 \times \left({(n_{i,o} - n_{i,t})}/{n_{i,o}} \right)$, i = reactants, t = reaction time.

$S_i = 100 \times \left({n_{i,t}}/{\sum_{i=1}^{n} n_{i,t}} \right)$, i = reactants, n = products, t = reaction time.

*Quantities for conversion and selectivity were determined by GC-FID analysis.

Finally, time-dependent compositional profiles were used to analyze the presented reaction pathway using the first- and second-rank Delplots approach.(77) The initial rates of cyclohexylamine and phenol conversion (r^0_i, mmol/h/mmol Pd) were obtained via polynomial regression and differentiation of the C_i vs. time curves (**Fig. 8a**), extrapolated to zero time. The results indicate that the amine is converted more rapidly (r^0_{CyA} = 7.5 h^{-1}) than phenol (r^0_{CyA} = 6.7 h^{-1}), presumably owing to its participation in the cyclohexanone condensation and its self-condensation. In addition, the concentration profile of the imine shows an intermediate-like behavior, with a maximum at 310 min. The eventual formation of the secondary amines (dicyclohexylamine and cyclohexylaniline) suggests their role as secondary products. However, the dicyclohexylamine profile should be carefully analyzed, as it could also suggest its role as an intermediary for the formation of cyclohexylaniline. This last point is discussed here based on the Delplots rank curves.

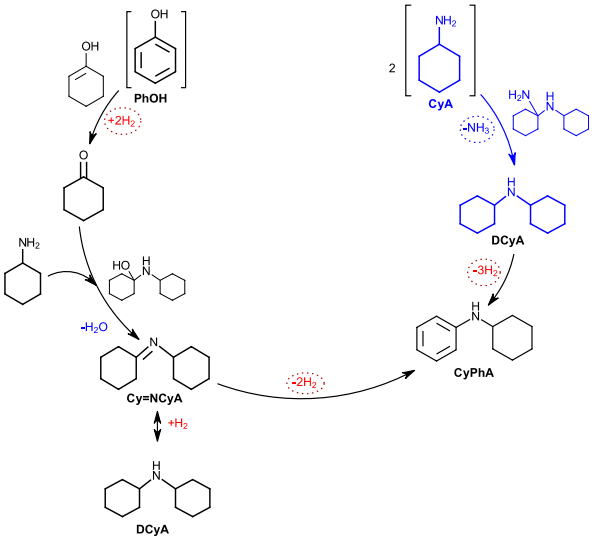

Figure 7. Proposed reaction pathway for the phenol-to-secondary amines reaction on Pd/C.

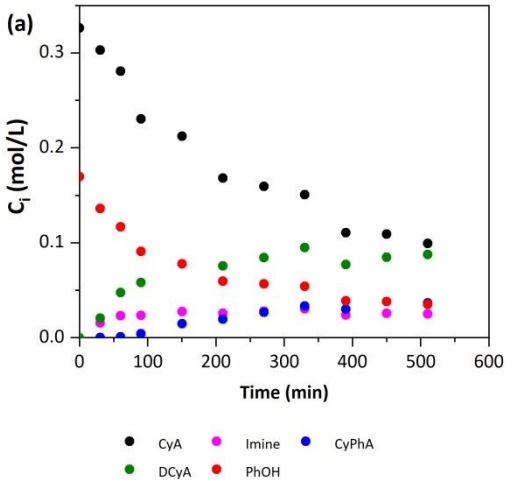

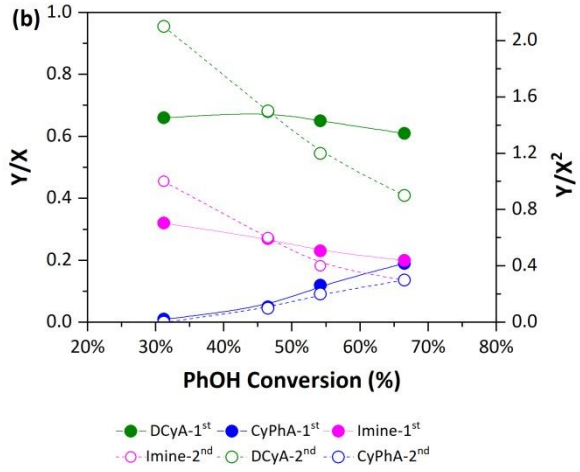

View Article Online
DOI: 10.1039/D2RE00259K

Figure 8. (a) Dynamic composition profiles for phenol reductive amination. (b) Delplots for the reaction products (the solid lines/solid symbols and dashed lines/hollow symbols corresponds to the first-rank and second-rank Delplots, respectively). The reaction experiments were performed at T = 140 °C with 0.2 mol/L phenol, 1.4 eq. cyclohexylamine, 1.5 bar H_2, 5% mol/mol Pd, and a reaction volume of 15 mL. PhOH: phenol; CyA: cyclohexylamine; DCyA: dicyclohexylamine; CyPhA: cyclohexylaniline.

According to the first-rank Delplots profiles for the reaction products (**Fig. 8b**), imine and dicyclohexylamine have finite Y-intercepts at zero time that correspond to primary products formed via parallel reactions taking place at different rates,(77) while cyclohexylaniline has a zero intercept that represents a high-order product. This indicates that dicyclohexylamine can be formed as a primary product via the reactions of self-condensation and with phenol (as previously discussed), while cyclohexylaniline is formed in a second reaction step. For the second-rank Delplots (**Fig. 8b**), the profiles for imine and dicyclohexylamine are similar and show a tendency to diverge in the Y-axis when X→0, which is characteristic of primary products. The curve for cyclohexylaniline confirms its role as a second-order product with a zero intercept on the Y-axis. The consistency between the product composition results, individual reactions for hydrogenation and self-condensation, and DelPlots analysis validates the reaction pathway proposed here. In the following sections, the effects of the catalyst support and metal nanoparticle size are assessed considering this reaction pathway.

Effect of catalyst support

The effect of the nature of the support on the catalytic amination of phenol with cyclohexylamine over Pd-based catalysts was studied for the Pd/Al_2O_3-D3, Pd/C, and Pd/SiO_2 catalysts. The supports were selected based on their differences in total acidity, density, and nature of acidic sites as well as their potential industrial applications.(16,31) Chen *et al*.(78) reported that the character of the support is relevant for the hydrogenation of phenol, in which both phenol and hydrogen adsorb on the metal sites.

The results of conversion, selectivity, and yields of secondary amines, as well as the acidic site densities of Pd/Al_2O_3-D3, Pd/C, and Pd/SiO_2 demonstrated that phenol conversion and yield of secondary amines were strongly favored by highly acidic catalysts (**Figs. 8a** and **8b**). Moreover, the imine is formed regardless of the nature of the support, which is consistent with previous findings.(19,79) The conversion values for Pd/Al_2O_3-D3 and Pd/C were 5 times higher than that for Pd/SiO_2, and the yield to secondary amines increased from 13% for Pd/SiO_2 to 64 and 82% for Pd/C and Pd/Al_2O_3-D3, respectively. In addition, different product distributions were observed among these catalysts, which could be related to the promotion or suppression of different reaction steps in the catalytic cycle owing to the density and/or nature of the acidic sites. These differences can be explained by the mechanistic divergences created over different types of acidic sites. Neri *et al*.(80) proposed that phenol adsorption is sensitive to the number of strong acidic and basic sites around the metal sites. In general, a support with a high phenol adsorption capacity will enhance phenol conversion, and cyclohexanone selectivity is increased owing to the weak interaction with the support.

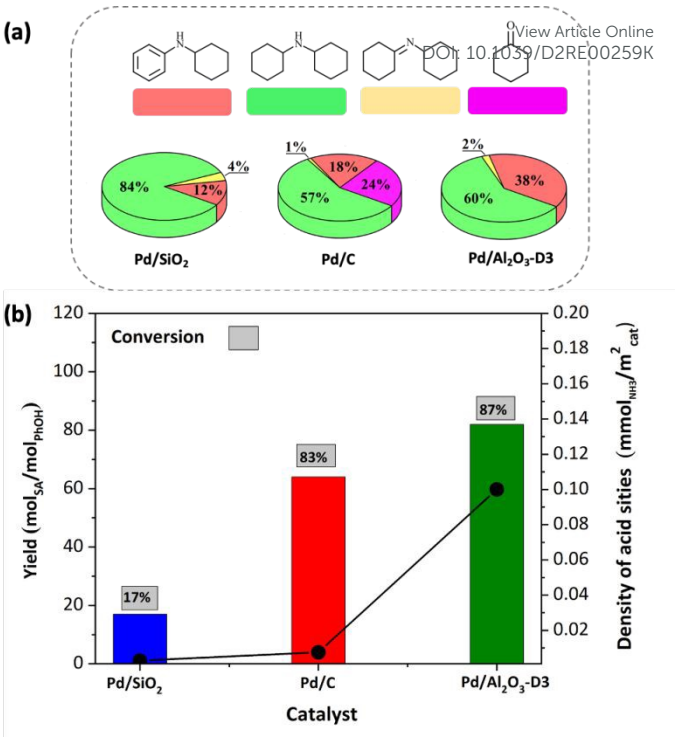

Figure 9. Effect of the catalyst support on phenol amination with cyclohexylamine. The reaction experiments were performed at T = 140 °C and with 0.2 mol/L phenol, 1.4 eq. cyclohexylamine, 1.5 bar H_2, and 5% mol/mol Pd.

Additional dynamic experiments were performed to estimate the initial reactant conversion and product formation rates. The rates (r^0_i, $mmol_i/h/mmol_{Pd}$) were calculated via polynomial regression and differentiation of the C_i vs. time curves extrapolated to zero time:

$$r_i^0 = \left[\left(\frac{1}{w_{Cat} * \frac{x_{Pd}}{MW_{Pd}} * D}\right)\left(\frac{dC_i}{dt}\right)\right]_{t=0} \quad (4)$$

The results (**Table 3**) indicate that the initial reaction rates for dicyclohexylamine formation and phenol consumption corresponding to the catalysts with different supports follow the order r^0_i (Pd/Al_2O_3-D3) >> r^0_i (Pd/C) > r^0_i (Pd/SiO_2). The low activity of Pd/SiO_2 can be explained by the weak adsorption of cyclohexylaniline and phenol, which hinders the elementary steps of the catalytic cycle. This could be caused by the weak acidity of this support with respect to those of carbon and Al_2O_3.

Table 3. Initial reaction rates for the individual reaction steps (as turnover frequency (TOF) values). Reaction conditions: T = 140 °C, 0.2 mol/L phenol (PhOH), 1.4 eq. Cyclohexylamine (CyA), 1.5 bar H_2, 5% mol Pd, and reaction volume = 15 mL. Ph=NCyA: cyclohexaneimine; DCyA: dicyclohexylamine.

Reaction	Pd/Al_2O_3-D3 TOF (h^{-1})	Pd/C TOF (h^{-1})	Pd/SiO_2 TOF (h^{-1})
PhOH + CyA + $2H_2$ → Ph=NCyA + H_2O	8.25	6.75	2.25
2CyA → DCyA + NH_3	11.25	6.75	4.5

The hydrogenation reactions on Pd-based catalysts proceed via a metal hydride ($^{H}Pd^{H}$) formed by the dissociation of H_2 on the Pd nanoparticles, which is a key step in the catalytic cycle.(18) However, because all the catalysts discussed in this section have the same metal loadings and similar dispersions, the rates of $^{H}Pd^{H}$ formation on their surfaces under a constant H_2 pressure are expected to be similar. Therefore, this step cannot explain the different conversions and product distributions. A theory that could explain this was proposed by Hattari and Shishida(21) and further confirmed by Vidal *et al.*,(17) who proposed the formation of protonic acidic sites via H spillover from $^{H}Pd^{H}$ to the Lewis acid sites of the support. Furthermore, Lewis acid sites can activate aromatic rings to become highly nucleophilic through electrophilic aromatic substitution reactions,(81) which induces the aromatic ring to accept electrophilic groups, such as H^+. The synergy of the metallic hydrogen activation(82) and Lewis acid sites can thus increase phenol conversion.

The high conversions and yields of secondary amines obtained for Pd/C and Pd/Al_2O_3-D3 suggest that the imine is formed and further hydrogenated preferentially on highly acidic materials. The enhanced imine hydrogenation can be attributed to the promotion of the condensation reaction on Lewis acid sites(17,19) and to the dragging effect of the hydrogenation/dehydrogenation reaction on imine formation.(22) The latter is a plausible explanation for the presence of cyclohexanone in the Pd/C products, whereas the cyclohexanone was completely condensed when Pd/Al_2O_3-D3 was used. Moreover, the two-fold increment in cyclohexylaniline selectivity found in Pd/Al_2O_3-D3 with respect to Pd/C suggests that the imine is adsorbed with different strengths, leading to a higher rate of hydrogenation/dehydrogenation on Pd/Al_2O_3-D3 than on Pd/C.

The previously discussed results allow us to conclude that the Lewis acidity of the catalysts followed the order Pd/Al_2O_3-D3 > Pd/C > Pd/SiO_2 and played an important role in the activity of the catalysts (**Fig. 9**), promoting the conversion of phenol and leading to high selectivity values of secondary amines. These results demonstrate that Pd offers hydrogenation sites, whereas the supports provide Lewis acid sites, which could enable H_2 spillover and enhance the hydrogenation of surface intermediates such as the imine.

Effect of the metal nanoparticle size

The effects of the metal nanoparticle size and dispersion on the catalytic performance were investigated using four catalysts with different particle sizes (1.7–7.7 ± 0.5 nm). In this particle size range, different metallic sites can be present in the particles, namely, terrace, corner, edge, and step sites. The rates (as TOF values, h^{-1}) of phenol amination with cyclohexylamine for the Pd/Al_2O_3-D1 (D=65%), Pd/Al_2O_3-D2 (D=48%), Pd/Al_2O_3-D3 (D =31%), and Pd/Al_2O_3-D4 (D=14%) catalysts increased with decreasing particle size, demonstrating the structural sensitivity of the reaction (**Fig. 10a**). The theoretical distribution of the facet, edge, and corner sites in these catalysts (**Fig. 10b**) was calculated using the method described by Le Valant *et al.*(24) and assuming an octahedral structure for the Pd particles, as observed via HRTEM. The combination of the site distribution with the TOF values demonstrates that phenol amination is favored on catalysts with a high proportion of low surface coordination Pd sites (17,19,25).

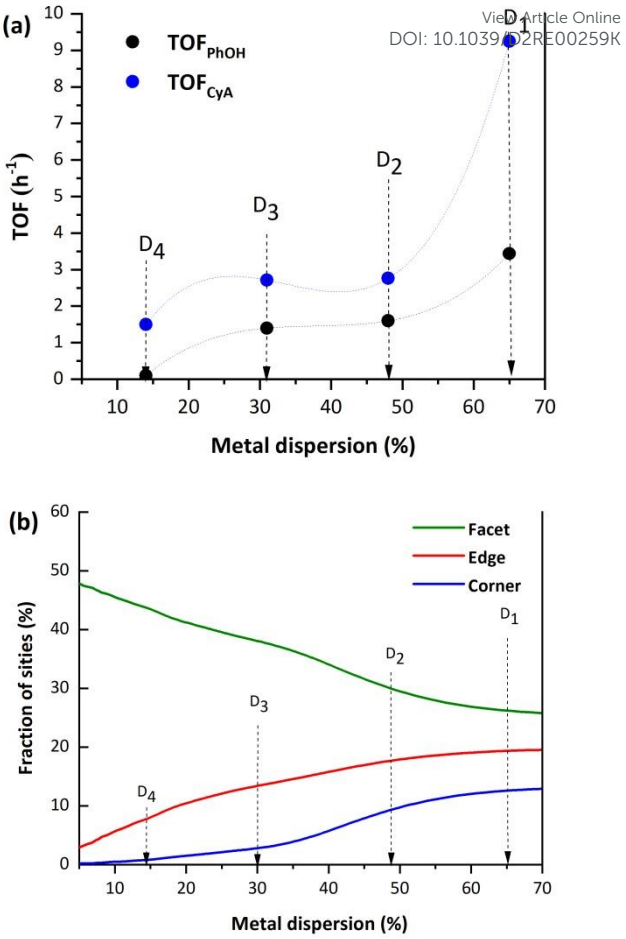

Figure 10. a) Effect of the metal dispersion on the turnover frequency (TOF). b) Fractions of different metal sites as functions of the metal dispersion.(83) The reaction experiments were carried out at T = 140 °C and with 0.2 mol/L phenol (PhOH), 1.4 eq. cyclohexylamine (CyA), 1.5 bar H_2, and 5% mol/mol Pd.

For structure-sensitive reactions, the nature of the activated chemical bond determines the arrangement of surface atoms that provides the lowest activation energy. However, the structural sensitivities of some reactions can be complementary depending on whether a bond is broken or formed. In fact, the TOF vs. D profiles shown here are similar to those reported by Van Santen(27) for reactions with complimentary dissociative bond cleavage and associative bond formation (Type I and Type III). The implications of the metal nanoparticle size for the elementary hydrogenation and amination steps in the phenol-to-secondary amines catalytic cycle are discussed next.

The first step in the phenol amination (PhOH→CyO) involves the partial hydrogenation of phenol via the conversion of -OH to C=O (**Fig. 11**). Mortensen *et al.*(84) measured an increase in the reaction rate upon increasing the metal particle size, presumably because benzene ring hydrogenation is fast on large facets, while phenol is adsorbed on the support. However, the effect of the support (especially for metal oxides) on phenol hydrogenation was several orders of magnitude greater than that of the particle size, which could explain the apparent contradiction with our results. Accordingly, our results can be explained by the high availability of $^{H}Pd^{H}$ sites for small particle sizes, which increases the probability of

H spillover to the support, generating extra Lewis acid sites. These sites are necessary for the conversion of phenol into a keto-enol intermediate and further isomerization to cyclohexanone, which explains the increase in phenol conversion TOF for low particle sizes.

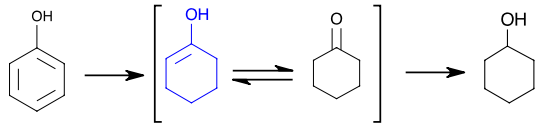

Figure 11. Reaction scheme for phenol hydrogenation on Pd/Al_2O_3.(85)

In the second step (imine → secondary amines), the C=N bond must be activated to facilitate imine hydrogenation/dehydrogenation. In this case, the activity increases with the fraction of low-coordination sites (steps and corners), which are reported to be chemoselective for C=N conversion.(17,19)

The previously discussed results indicate that high proportions of low-coordination sites in the Pd/Al_2O_3 catalysts increase their effectiveness in phenol amination. Therefore, a direct characterization of the surface was performed via CO adsorption experiments on Pd/Al_2O_3-D1, Pd/Al_2O_3-D2, Pd/Al_2O_3-D3, and Pd/Al_2O_3-D4. The experiments were conducted using diffuse reflectance infrared spectroscopy with Fourier transform (DRIFTS) on a Nicolet iS50 infrared spectrometer (Thermo Scientific) interfaced with a mass spectrometer (Pfeiffer QMG 220).

Figure 12 shows the IR spectrum at 30 °C after performing the CO adsorption experiments for the reduced Pd/Al_2O_3 catalysts (D1 to D4). The IR band at 2082 cm^{-1} was detected for all the catalyst samples and was attributed to CO molecules linearly adsorbed on metallic Pd.(19,86) This linear adsorption is characteristic of Pd particles with facets (111) and low-coordination Pd atoms (edges and corners), which is consistent with the low range of particle sizes obtained here (< 10 nm).(87,88) In addition, the intense signals at 1976 and 1926 cm^{-1} (more pronounced on catalysts with large nanoparticles) correspond to the bridge CO and three-fold CO configurations, which are commonly located at terrace sites in Pd (100), (110), and (111).(19,87,89,90) Accordingly, the intensity ratios of these signals, $\left({a_{2082}}/{(a_{1976}+a_{1926})}\right)$ are proportional to the fractions of uncoordinated sites in the catalysts, which follow the order Pd/Al_2O_3-D1 (0.184) > Pd/Al_2O_3-D2 (0.151) > Pd/Al_2O_3-D3 (0.136) > Pd/Al_2O_3-D4 (0.106) (See insert in Fig. 12). Therefore, based on the CO IR and HRTEM results and the catalytic data gathered here, we confirmed that catalysts with a high proportion of uncoordinated Pd sites, such as Pd/Al_2O_3-D1, are likely to favor phenol amination.

Conclusions

Phenol amination is a multistep process that begins with phenol hydrogenation controlled by the primary hydrogenation of phenol to cyclohexanone and by the activation of C=N bonds in the intermediate imine. The imine is formed regardless of the nature of the catalyst or support. However, its hydrogenation/dehydrogenation into secondary amines is enhanced by the presence of Lewis acid sites. Such sites are provided by the support or formed via the spillover of H from $^{H}Pd^{H}$ to the support. In addition, the metal particle size analysis demonstrated that phenol amination is a structure-sensitive reaction favored by the presence of low-coordination Pd sites. The former was demonstrated by a six-fold increase in the TOF (h^{-1}) upon a particle dispersion increase from 14% (Pd/Al_2O_3-D4) to 64% (Pd/Al_2O_3-D1). Moreover, the DRIFTS-CO surface characterization demonstrated a high proportion of low-coordination sites on the Pd/Al_2O_3-D1 catalyst.

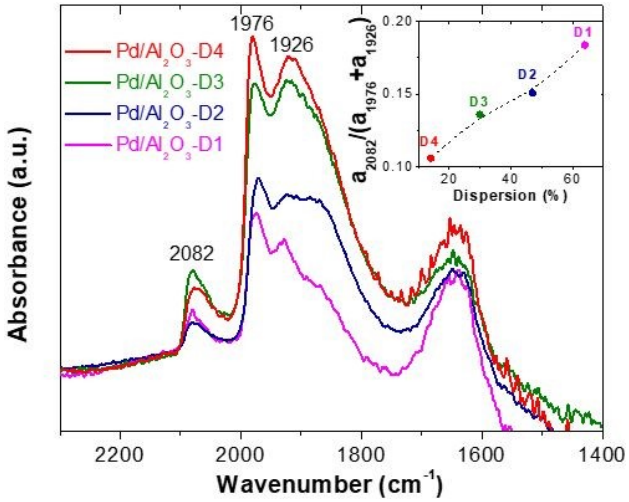

Figure 12. Diffuse reflectance infrared spectroscopy with Fourier transforms spectra of adsorbed CO on supported Pd catalysts at 200°C. **Note:** Analysis performed after catalysts reduction.

Author Contributions

Conceptualization: Luis E. Arteaga and Romel Jimenez. *Methodology*: Maray Ortega, Raydel Manrique, and Julieth García. *Formal analysis and investigation*: Maray Ortega, Guillermo Reyes, and Raydel Manrique. *Writing - original draft preparation*: Maray Ortega and Daviel Gómez. *Writing - review and editing*: Luis E. Arteaga, Romel Jiménez, and Victor Baldovino. *Project administration*: Luis E. Arteaga.

Conflicts of interest

The authors declare that they have no known competing financial interests or personal relationships that could have influenced the work reported in this study.

Acknowledgements

The authors would like to thank FONDECYT Grant 1190063, ACE Grant 210012, 2260311 AD/EQ and FONDEQUIP EQM Grant170077 for their financial support.

References

1. Segobia DJ, Trasarti AF, Apesteguía CR. Selective one-pot synthesis of asymmetric secondary amines via N-alkylation of nitriles with alcohols. J Catal. 2019;380:178–85.

2. Salvatore RN, Nagle AS, Kyung WJ. Cesium effect: High

chemoselectivity in direct N-alkylation of amines. J Org Chem. 2002;67(3):674–83.

3. Tamboli AH, Chaugule AA, Sheikh FA, Chung WJ, Kim H. Synthesis, characterization, and application of silica supported ionic liquid as catalyst for reductive amination of cyclohexanone with formic acid and triethyl amine as hydrogen source. Chinese J Catal. 2015;36(8):1365–71.

4. Zhong J, Wei YS, Wan HF, Wu YL, Zheng JX, Han SH, et al. Greenhouse gas emission from the total process of swine manure composting and land application of compost. Atmos Environ. 2013;81:348–55.

5. Shimizu KI, Imaiida N, Kon K, Hakim Siddiki SMA, Satsuma A. Heterogeneous Ni catalysts for N-alkylation of amines with alcohols. ACS Catal. 2013;3(5):998–1005.

6. Nakamura Y, Kon K, Touchy AS, Shimizu KI, Ueda W. Selective synthesis of primary amines by reductive amination of ketones with ammonia over supported Pt catalysts. ChemCatChem. 2015;7(6):921–4.

7. Shimizu KI, Kon K, Onodera W, Yamazaki H, Kondo JN. Heterogeneous Ni catalyst for direct synthesis of primary amines from alcohols and ammonia. ACS Catal. 2013;3(1):112–7.

8. Taniguchi K, Jin X, Yamaguchi K, Nozaki K, Mizuno N. Versatile routes for synthesis of diarylamines through acceptorless dehydrogenative aromatization catalysis over supported gold–palladium bimetallic nanoparticles. Chem Sci. 2017;8(3):2131–42.

9. Koizumi Y, Taniguchi K, Jin X, Yamaguchi K, Nozaki K, Mizuno N. Formal arylation of NH3 to produce diphenylamines over supported Pd catalysts. Chem Commun. 2017;53(78):10827–30.

10. Cuypers T, Tomkins P, De Vos DE. Direct liquid-phase phenol-to-aniline amination using Pd/C. Catal Sci Technol. 2018;8(10):2519–23.

11. Chen Z, Zeng H, Girard SA, Wang F, Chen N, Li CJ. Formal Direct Cross-Coupling of Phenols with Amines. Angew Chemie - Int Ed. 2015;54(48):14487–91.

12. Tomkins P, Valgaeren C, Adriaensen K, Cuypers T, De Vos DE. The impact of the nature of amine reactants in the palladium catalyzed conversion of phenol to N-substituted anilines. J Catal. 2019;371:207–13.

13. Jameel F, Stein M. The Many Roles of Solvent in Homogeneous Catalysis - The Reductive Amination Showcase. J Catal 2021, . 2021 Nov;405:24–34.

14. Chen Z, Zeng H, Gong H, Wang H, Li C-J. Palladium-catalyzed reductive coupling of phenols with anilines and amines: efficient conversion of phenolic lignin model monomers and analogues to cyclohexylamines. Chem Sci. 2015;6(7):4174–8.

15. Tomkins P, Valgaeren C, Adriaensen K, Cuypers T, Vos DE De. The Rhodium Catalysed Direct Conversion of Phenols to Primary Cyclohexylamines. ChemCatChem. 2018;10:3689–93.

16. Cuypers T, Morias T, Windels S, Marquez C, Van Goethem C, Vankelecom I, et al. Ni-Catalyzed reductive amination of phenols with ammonia or amines into cyclohexylamines. Green Chem. 2020;22(6):1884–93.

17. Vidal JD, Climent MJ, Concepcion P, Corma A, Iborra S, Sabater MJ. Chemicals from Biomass: Chemoselective Reductive Amination of Ethyl Levulinate with Amines. ACS Catal. 2015;5(10):5812–21.

18. Corma A, Ródenas T, Sabater MJ. A bifunctional PdVMgO solid catalyst for the one-pot selective N-monoalkylation of amines with alcohols. Chem - A Eur J. 2010;16(1):254–60.

19. Mazarío J, Raad Z, Concepción P, Cerdá-Moreno C, Domine ME. Pd supported on mixed metal oxide as an efficient catalyst for the reductive amination of bio-derived acetol to 2-methylpiperazine. Catal Sci Technol. 2020;10(23):8049–63.

20. Resende KA, Hori CE, Noronha FB, Shi H, Gutierrez OY, Camaioni DM, et al. Aqueous phase hydrogenation of phenol catalyzed by Pd and PdAg on ZrO2. Appl Catal A Gen. 2017 Nov;548:128–35.

21. Hattori H, Shishido T. Molecular hydrogen-originated protonic acid site as active site on solid acid catalyst. Catal Surv from Japan. 1997;1(2):205–13.

22. Santoro F, Psaro R, Ravasio N, Zaccheria F. Reductive amination of ketones or amination of alcohols over heterogeneous cu catalysts: Matching the catalyst support with the n-alkylating agent. ChemCatChem. 2012;4(9):1249–54.

23. Gomez S, Peters JA, Maschmeyer T. The Reductive Animation of Aldehydes and Ketones and the Hydrogenation of Nitriles: Mechanistic Aspects and Selectivity Control. Adv Synth Catal. 2002;344(10):1037–57.

24. Le Valant A, Drault F, Maleix C, Comminges C, Beauchet R, Batonneau Y, et al. Effect of the metallic particle size of supported Pt catalysts on methylcyclopentane hydrogenolysis: Understanding of the ring opening products distribution by a geometric approach. J Catal. 2018;367:234–43.

25. Zhao M, Shi J, Hou Z. Selective hydrogenation of phenol to cyclohexanone in water over Pd catalysts supported on Amberlyst-45. Chinese J Catal. 2016;37(2):234–9.

26. Soled S, Malek A, Miseo S, Baumgartner J, Kliewer C, Afeworki M, et al. Supported metal catalysts: Some interesting new leads in an old field. Stud Surf Sci Catal. 2006;162:103–10.

27. Van Santen RA. Complementary structure sensitive and insensitive catalytic relationships. Acc Chem Res. 2009;42(1):57–66.

28. Patterson AL. The Scherrer Formula for X-Ray Particle Size Determination. Phys Rev. 1939 Nov;56(10):978–82.

29. Vannice MA. Kinetics of Catalytic Reactions. Boston, MA: Springer US; 2005.

30. Cuypers T, Tomkins P, De Vos DE. Direct liquid-phase phenol-to-aniline amination using Pd/C. Catal Sci Technol. 2018 May;8(10):2519–23.

31. Rong Y, Ji N, Yu Z, Diao X, Li H, Lei Y, et al. Lignin amination valorization: heterogeneous catalytic synthesis of aniline and benzylamine from lignin-derived chemicals. Green Chem. 2021;23(18):3.

32. Manrique Suárez R, Ortega Díaz M, Jiménez Concepción R, Arteaga Pérez LE, Casas Y. Data for: Production of secondary amines through the catalytic reductive amination of biomass-derived phenol with cyclohexylamine over carbon-supported palladium and rhodium catalysts [Internet]. Mendeley Data. Mendeley Data V1: Mendeley Data V1; 2022. p. 10.17632/z5bypjm62y.1. Available from: https://data.mendeley.com/datasets/z5bypjm62y

33. Batista J, Pintar A, Mandrino D, Jenko M, Martin V. XPS and TPR examinations of γ-alumina-supported Pd-Cu catalysts. Appl Catal A Gen. 2001;206(1):113–24.

34. Li H, Sun G, Jiang Q, Zhu M, Sun S, Xin Q. Preparation and characterization of Pd/C catalyst obtained in NH3-mediated polyol process. J Power Sources. 2007;172(2):641–9.

35. Pinna F, Menegazzo F, Signoretto M, Canton P, Fagherazzi G, Pernicone N. Consecutive hydrogenation of benzaldehyde over Pd catalysts: Influence of supports and sulfur poisoning. Appl Catal A Gen. 2001;219(1):195–200.

36. Menegazzo F, Fantinel T, Signoretto M, Pinna F. Metal dispersion and distribution in Pd-based PTA catalysts. Catal Commun. 2007;8(6):876–9.

37. ZHOU Z liang, JI S fu, YIN F xiang, LU Z xiang, LI C yue. Preparation of Pd/CexZr1-xO2/SiO2 and its catalyticperformance in methane combustion. J Fuel Chem Technol. 2007 Oct;35(5):583–8.

38. Segobia DJ, Trasarti AF, Apesteguía CR. Hydrogenation of nitriles to primary amines on metal-supported catalysts: Highly selective conversion of butyronitrile to n-butylamine. Appl Catal A Gen. 2012 Nov;445–446:69–75.

39. Sitthisa S, Pham T, Prasomsri T, Sooknoi T, Mallinson RG, Resasco DE. Conversion of furfural and 2-methylpentanal on Pd/SiO2 and Pd–Cu/SiO2 catalysts. J Catal. 2011 May;280(1):17–27.

40. Sepúlveda JH, Fígoli NS. The influence of calcination temperature on Pd dispersion and hydrogen solubility in Pd/SiO2. Appl Surf Sci. 1993 Jun;68(2):257–64.

41. Corma A, García H. Lewis Acids: From Conventional Homogeneous to Green Homogeneous and Heterogeneous Catalysis. Chem Rev. 2003 Nov;103(11):4307–65.

42. Sheng L, Ma Z, Chen S, Lou J, Li C, Li S, et al. Mechanistic insight into N2O formation during NO reduction by NH3 over Pd/CeO2 catalyst in the absence of O2. Chinese J Catal. 2019 Jul;40(7):1070–7.

43. Wang P, Zhang M, Zhang W, Yang C, Li C. Consequence of heterogeneity of active sites for reactivity mechanism of n-butane isomerization over SO42−/ZrO2-Al2O3 catalyst. Appl Catal A Gen. 2017 Jul;542:311–6.

44. Li P, Zhang R, Liu N, Royer S. Efficiency of Cu and Pd substitution in Fe-based perovskites to promote N2 formation during NH3 selective catalytic oxidation (NH3-SCO). Appl Catal B Environ. 2017 Apr;203:174–88.

45. Zhou H, Ge MY, Wu S, Ye B, Su Y. Iron based monolithic catalysts supported on Al2O3, SiO2, and TiO2: A comparison for NO reduction with propane. Fuel. 2018 May;220:330–8.

46. Tong Z, Li X, Zhu J, Chen S, Dai G, Deng Q, et al. Iodine-Modified Pd Catalysts Promote the Bifunctional Catalytic Synthesis of 2,5-Hexanedione from C6 Furan Aldehydes. ChemSusChem. 2021;e202102444.

47. Weng Z, Zaera F. Sub-Monolayer Control of Mixed-Oxide Support Composition in Catalysts via Atomic Layer Deposition: Selective Hydrogenation of Cinnamaldehyde Promoted by (SiO2-ALD)-Pt/Al2O3. ACS Catal. 2018 Sep;8(9):8513–24.

48. Cao Q, Zhang W, Luo S, Guo R, Xu D. Synthesis of Furanic Ethers from Furfuryl Alcohol for Biofuel Production. Energy and Fuels. 2021 Aug;35(15):12725–33.

49. Castaño P, Pawelec B, Fierro JLG, Arandes JM, Bilbao J. Enhancement of pyrolysis gasoline hydrogenation over Pd-promoted Ni/SiO2–Al2O3 catalysts. Fuel. 2007 Oct;86(15):2262–74.

50. Volckmar CE, Bron M, Bentrup U, Martin A, Claus P. Influence of the support composition on the hydrogenation of acrolein over Ag/SiO2–Al2O3 catalysts. J Catal. 2009 Jan;261(1):1–8.

51. Liu X. DRIFTS study of surface of γ-alumina and its dehydroxylation. J Phys Chem C. 2008 Apr;112(13):5066–73.

52. Emeis CA. Determination of Integrated Molar Extinction Coefficients for Infrared Absorption Bands of Pyridine Adsorbed on Solid Acid Catalysts. J Catal. 1993 Jun;141(2):347–54.

53. Wu Q, Zhang G, Gao M, Cao S, Li L, Liu S, et al. Clean production of 5-hydroxymethylfurfural from cellulose using a hydrothermal/biomass-based carbon catalyst. J Clean Prod. 2019 Mar;213:1096–102.

54. Wang L, Wu Q, Zhao B, Li Z, Zhang Y, Huang L, et al. Multi-functionalized carbon aerogels derived from chitosan. J Colloid Interface Sci. 2022 Jan;605:790–802.

55. Ryczkowski J. IR spectroscopy in catalysis. Catal Today. 2001 Jul;68(4):263–381.

56. Wang W, Dong Y, Xu L, Dong W, Niu X, Lei Z. Combining Bimetallic-Alloy with Selenium Functionalized Carbon to Enhance Electrocatalytic Activity towards Glucose Oxidation. Electrochim Acta. 2017 Aug;244:16–25.

57. Xu H, Yan B, Zhang K, Wang C, Zhong J, Li S, et al. Facile synthesis of Pd-Ru-P ternary nanoparticle networks with enhanced electrocatalytic performance for methanol oxidation. Int J Hydrogen Energy. 2017 Apr;42(16):11229–38.

58. Benipal N, Qi J, Liu Q, Li W. Carbon nanotube supported PdAg nanoparticles for electrocatalytic oxidation of glycerol in anion exchange membrane fuel cells. Appl Catal B Environ. 2017 Aug;210:121–30.

59. Xiong R, Zhao W, Wang Z, Zhang M. A sulfur-tolerant phosphorus doped Pd/C catalyst for hydrogenation of 4-

nitrothioanisole. Mol Catal. 2021;500(August 2020):111332.

60. Graulis S, Chateigner D, Downs RT, Yokochi AFT, Quirós M, Lutterotti L, et al. Crystallography Open Database - An open-access collection of crystal structures. J Appl Crystallogr. 2009;42(4):726–9.

61. Simplício LMT, Brandão ST, Sales EA, Lietti L, Bozon-Verduraz F. Methane combustion over PdO-alumina catalysts: The effect of palladium precursors. Appl Catal B Environ. 2006 Mar;63(1–2):9–14.

62. Jiang H, Lin J, Wu X, Wang W, Chen Y, Zhang M. Efficient hydrogenation of CO2 to methanol over Pd/In2O3/SBA-15 catalysts. J CO2 Util. 2020 Feb;36:33–9.

63. Snyder RL, Fiala J, Bunge HJ. Defect and Microstructure Analysis by Diffraction. Oxford University Press, editor. Oxford; 1999. Vol. 200.

64. Zhang Z, Zhou F, Lavernia EJ. On the analysis of grain size in bulk nanocrystalline materials via x-ray diffraction. Metall Mater Trans A 2003 346. 2003;34(6):1349–55.

65. Kibasomba PM, Dhlamini S, Maaza M, Liu CP, Rashad MM, Rayan DA, et al. Strain and grain size of TiO2 nanoparticles from TEM, Raman spectroscopy and XRD: The revisiting of the Williamson-Hall plot method. Results Phys. 2018 Jun;9:628–35.

66. Leopold K, Maier M, Schuster M. Preparation and characterization of Pd/Al2O3 and Pd nanoparticles as standardized test material for chemical and biochemical studies of traffic related emissions. Sci Total Environ. 2008 May;394(1):177–82.

67. Fang G, Li W, Shen X, Perez-Aguilar JM, Chong Y, Gao X, et al. Differential Pd-nanocrystal facets demonstrate distinct antibacterial activity against Gram-positive and Gram-negative bacteria. Nat Commun 2018 91. 2018 Jan;9(1):1–9.

68. Zhang D, Jin C, Tian H, Xiong Y, Zhang H, Qiao P, et al. An In situ TEM study of the surface oxidation of palladium nanocrystals assisted by electron irradiation. Nanoscale. 2017 May;9(19):6327–33.

69. Demidova YS, Simakova IL, Wärnå J, Simakov A, Murzin DY. Kinetic modeling of one-pot myrtenol amination over Au/ZrO2 catalyst. Chem Eng J. 2014;238:164–71.

70. Nelson NC, Manzano JS, Sadow AD, Overbury SH, Slowing II. Selective Hydrogenation of Phenol Catalyzed by Palladium on High-Surface-Area Ceria at Room Temperature and Ambient Pressure. ACS Catal. 2015;5(4):2051–61.

71. Zhang H, Han A, Okumura K, Zhong L, Li S, Jaenicke S, et al. Selective hydrogenation of phenol to cyclohexanone by SiO2-supported rhodium nanoparticles under mild conditions. J Catal. 2018;364:354–65.

72. Arteaga-Pérez LE, Manrique R, Ortega M, Castillo-Puchi F, Fraile JE, Jiménez R. Elucidating the Role of Rh/C on the Pathways and Kinetics of Ketone-to-Secondary Amines Reaction. ChemCatChem. 2022;14:1–11.

73. Gunanathan C, Milstein D. Selective Synthesis of Primary Amines Directly from Alcohols and Ammonia. Science (80-). 2008;3:8789–92.

74. Domine ME, Hernández-soto MC, Pérez Y. Development of metal nanoparticles supported materials as efficient catalysts for reductive amination reactions using high-throughput experimentation. Catal Today. 2011;159(1):2–11.

75. Pelckmans M, Renders T, Van de Vyver S, Sels BF. Bio-based amines through sustainable heterogeneous catalysis. Green Chem. 2017;19(22):5303–31.

76. Hong Z, Ge X, Zhou S. Underlying Mechanisms of Reductive Amination on Pd-Catalysts : The Unique Role of Hydroxyl Group in Generating Sterically Hindered Amine. Int J Mol Sci. 2022;23:7621.

77. Bhore NA, Klein MT, Bischoff KB. The Delplot Technique: A New Method for Reaction Pathway Analysis. Ind Eng Chem Res. 1990;29(2):313–6.

78. Chen H, Sun J. Selective hydrogenation of phenol for cyclohexanone: A review. J Ind Eng Chem. 2021;94(92):78–91.

79. Arteaga-Pérez LE, Manrique R, Castillo-Puchi F, Ortega M, Bertiola C, Pérez A, et al. One-pot amination of cyclohexanone-to-secondary amines over carbon-supported Pd: Unraveling the reaction mechanism and kinetics. Chem Eng J. 2021;417:129236.

80. Neri G, Visco AM, Donato A, Milone C, Malentacchi M, Gubitosa G. Hydrogenation of phenol to cyclohexanone over palladium and alkali-doped palladium catalysts. Appl Catal A Gen. 1994 Mar;110(1):49–59.

81. Deshmukh RR, Lee JW, Shin US, Lee JY, Song CE. Hydrogenation of Arenes by Dual Activation: Reduction of Substrates Ranging from Benzene to C60 Fullerene under Ambient Conditions. Angew Chemie. 2008 Oct;120(45):8743–5.

82. Benkhaled M, Descorme C, Duprez D, Morin S, Thomazeau C, Uzio D. Study of hydrogen surface mobility and hydrogenation reactions over alumina-supported palladium catalysts. Appl Catal A Gen. 2008 Aug;346(1–2):36–43.

83. Benfield RE. Mean coordination numbers and the non-metal-metal transition in clusters. J Chem Soc Faraday Trans. 1992;88(8):1107–10.

84. Sio N, Mortensen PM, Grunwaldt J, Jensen PA, Jensen AD. Influence on nickel particle size on the hydrodeoxygenation of phenol. Catal Today. 2016;259:277–84.

85. Liu H, Jiang T, Han B, Liang S, Zhou Y. Selective phenol hydrogenation to cyclohexanone over a dual supported Pd-Lewis acid catalyst. Science (80-). 2009;326(5957):1250–2.

86. Busca G, Finocchio E, Escribano VS. Infrared studies of CO oxidation by oxygen and by water over Pt/Al2O3 and Pd/Al2O3 catalysts. Appl Catal B Environ. 2012 Feb;113–114:172–9.

87. Pitchon V, Primet M, Praliaud H. Alkali addition to silica-supported palladium: Infrared investigation of the carbon monoxide chemisorption. Appl Catal. 1990 Jun;62(1):317–34.

88. Liotta LF, Martin GA, Deganello G. The Influence of Alkali

View Article Online
DOI: 10.1039/D2RE00259K

Metal Ions in the Chemisorption of CO and CO2on Supported Palladium Catalysts: A Fourier Transform Infrared Spectroscopic Study. J Catal. 1996 Dec;164(2):322–33.

89. Dulaurent O, Chandes K, Bouly C, Bianchi D. Heat of Adsorption of Carbon Monoxide on a Pd/Al2O3 Solid Using in Situ Infrared Spectroscopy at High Temperatures. J Catal. 1999 Dec;188(2):237–51.

90. Pavlova SN, Sadykov VA, Razdobarov VA, Paukshtis EA. The Influence of Support on the Low-Temperature Activity of Pd in the Reaction of CO Oxidation: 2. Adsorption Properties and Reactivity of Adsorbed Species. J Catal. 1996 Jul;161(2):507–16.